ACS APPLIED NANO MATERIALS

www.acsanm.org Article

Surface Air Plasma Treatment of Laser-Induced Graphene-Based Electrodes for Enhanced Electrochemical Sensing Performance

Saumik Dey Shovan, Shapour Jafargholinejad, Mohamad Kannan Idris, Carlos Rodríguez Perales, Aamir Minhas-Khan, Pouya Rezai,* and Gerd Grau*

Cite This: *ACS Appl. Nano Mater.* 2025, 8, 17052−17064 Read Online

ACCESS | Metrics & More | Article Recommendations | Supporting Information

Downloaded via YORK UNIV on February 26, 2026 at 16:35:12 (UTC).
See https://pubs.acs.org/sharingguidelines for options on how to legitimately share published articles.

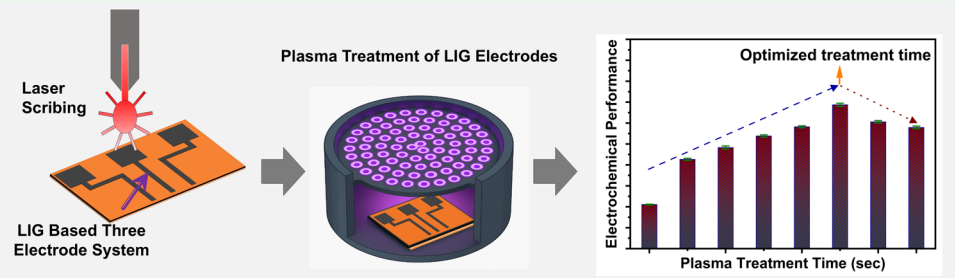

ABSTRACT: Laser-induced graphene (LIG) is a cost-effective and sustainable single-step electrode fabrication technique for electrochemical applications that eliminates the need for additional materials or complex processing. Plasma treatment has been applied to enhance the electrochemical performance of LIG electrodes. However, the effect of varying treatment durations on LIG performance remains unexplored, leaving a gap in understanding whether electrochemical properties improve gradually with increased exposure time. We investigate the effect of air plasma treatment time (0−120 s) on the electrochemical and material properties of LIG electrodes. Treatment intervals are set at 10 s from 0−60 s for detailed trend analysis, with an extended 120 s point. Cyclic voltammetry (CV) and material characterization techniques determine the optimal treatment time of the 50 s that enhances sensor performance by balancing increased surface reactivity with overexposure. Compared to untreated electrodes, the optimized electrodes exhibited a 243% increase in CV current, a 25-fold reduction in charge transfer resistance (R_{ct}) measured via electrochemical impedance spectroscopy (EIS), a 10-fold lower limit of detection (LOD) for potassium ferrocyanide/ferricyanide. Additionally, the treated sensors maintained stable performance over 14 days, demonstrating their long-term reliability. These findings highlight the importance of plasma treatment optimization in enhancing the performance of LIG-based electrochemical sensors.

KEYWORDS: *laser-induced graphene (LIG), plasma treatment, electrochemical sensing, limit of detection (LOD), potassium ferrocyanide/ferricyanide*

1. INTRODUCTION

As the demand for environmental monitoring and healthcare diagnostics continues to grow, the development of electrochemical sensors is increasingly focused on improving efficiency, affordability, detection limits, and durability to meet evolving research and industry needs. Electrochemical sensors provide a unique blend of accuracy and portability while offering key advantages such as simple sample preparation, selective detection, and rapid analysis.[1] Nowadays, screen-printed electrodes (SPE), glassy carbon electrodes (GCE), and paper-based analytical devices (ePADs) are commonly used electrode materials in electrochemical sensors due to their accessibility and practicality.[2,3] Carbon materials such as electrochemically reduced graphene oxide are employed as electrocatalysts, demonstrating significant potential in sensor performance.[4] Alongside these pristine carbon materials, metal−carbon composites have gained substantial research interest for their potential to enhance sensor performance. Composites like metal oxide-carbon (e.g., ZnO),[5] carbon-supported metals (e.g., palladium),[6] and conducting polymer-carbon blends (e.g., poly(3,4-ethylenedioxythiophene)-graphene (PEDOT-Gr))[7] bring unique properties that enhance the sensitivity and stability of electrochemical sensors.

While the above materials have demonstrated effectiveness, there is increasing interest in novel alternatives that offer

Received: May 16, 2025
Revised: August 15, 2025
Accepted: August 18, 2025
Published: August 22, 2025

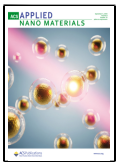

ACS Publications © 2025 American Chemical Society

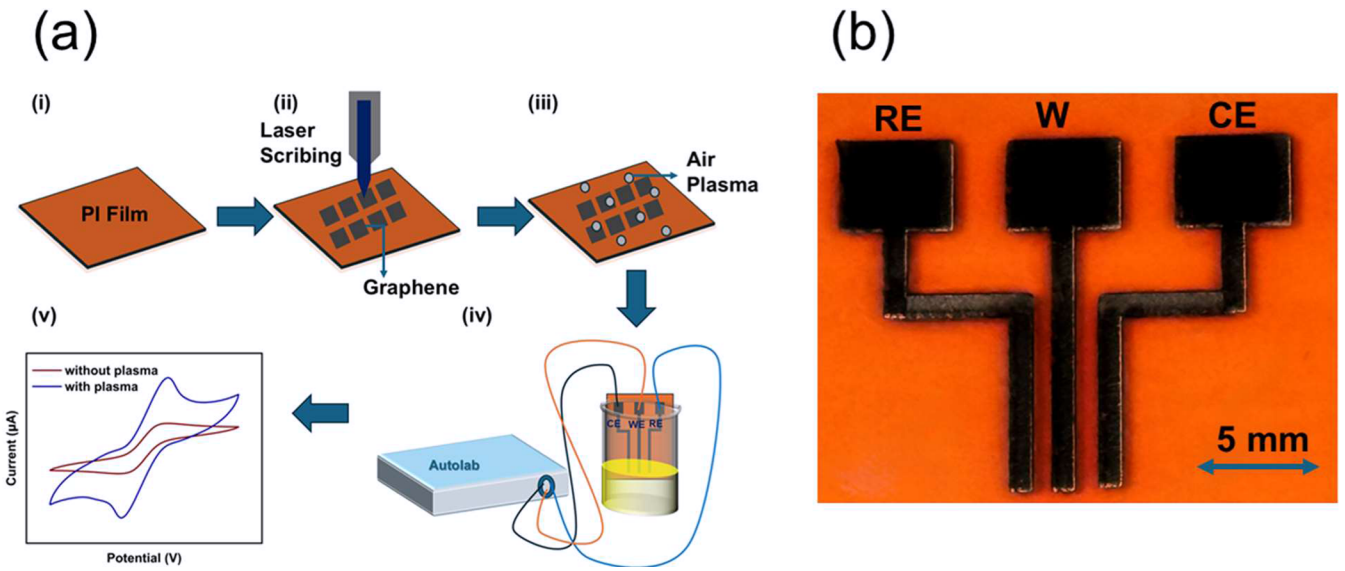

Figure 1. LIG electrodes fabricated for plasma oxidization and electrochemical testing. (a) Schematic of the fabrication process: (i) preparation of the polyimide film substrate, (ii) laser scribing for LIG formation, (iii) air plasma treatment of LIG electrodes to enhance surface properties, (iv) electrochemical testing setup for performance evaluation, (v) improved electrochemical performance observed through CV. (b) Optical micrograph of the fabricated LIG three-electrode system showing the RE, WE, and CE.

enhanced performance and greater scalability. One such alternative material is LIG, a material that leverages the unique properties of laser-induced carbonization.[8,9] LIG is a porous form of graphene with a large specific surface area, making it very promising for use as an electrode material for electrochemical devices such as supercapacitors.[10] It is an ideal candidate for disposable electrodes and has the potential to replace widely used electrode materials like SPE, GCE, and ePADs in electrochemical sensors.[11]

Compared to other electrode fabrication methods, LIG stands out due to its simplicity and cost-effectiveness. Unlike SPEs, which require specialized conductive inks and multiple fabrication steps, LIG only needs a carbon-based substrate and a commercially available laser system to convert the substrate into LIG in a single step, eliminating the need for additional materials.[12,10] Similarly, conductive polymer casting involves the synthesis and curing of materials, adding complexity, while ePADs are simple but lack the precision and versatility of LIG.[13,14] LIG's binder-free nature and minimal material wastage make it a more efficient, sustainable, and accessible option for producing intricate, high-performance carbon or graphene-based electrodes.

Recent studies have explored the use of LIG as an electrode material for electrochemical sensors. For instance, researchers have developed LIG-based electrochemical sensors for dopamine detection.[15] A LIG-based aptasensor was fabricated by coupling pyrenebutyric acid with a thrombin aptamer.[8] Additionally, lactate, potassium, and conductivity in sweat were measured using a LIG-based sensor through amperometry and potentiometry.[9] A microfluidic device with integrated microchannels and interdigitated electrodes was fabricated using LIG, enabling capacitive sensing for the detection of five human taste gustative perceptions.[11] More examples of LIG-based sensors are discussed in several review papers, highlighting their development and use in different areas.[16,17]

Despite their promising performance, LIG materials in these sensors face a critical challenge, i.e., their inherent hydrophobicity limits interaction with aqueous electrolytes, hindering electrochemical reactions.[18] This issue extends beyond LIG to other carbon-based and polymeric materials commonly used in sensing and energy storage applications, where surface wettability plays a crucial role in performance.[19−21] Plasma treatment offers a widely used and effective solution to this problem by modifying surface properties without altering the material's bulk structure.[22] Plasma generates high-energy ions and reactive surface functional groups that interact with surfaces, modifying their surface morphology and chemical functionality without destroying the bulk surface's integrity.[19] Compared to other surface activation methods such as piranha treatment or electrochemical activation in acidic media, plasma treatment presents distinct advantages. Piranha solution, while effective, is highly aggressive and unsuitable for polymer-based or microstructure substrates due to its potential to degrade or alter material surfaces.[23] Similarly, electrochemical activation in acidic media may not be appropriate when neutral or physiological pH conditions are required, especially for biosensing applications.[24] In contrast, plasma treatment is a dry, tunable, and environmentally friendly approach that enables selective surface functionalization. It effectively introduces hydrophilic groups to enhance wettability, while preserving the device's compatibility with sensitive materials and flexible substrates.

Previous studies have applied plasma treatment as a method for enhancing the performance of LIG in various applications. For instance, oxygen plasma treatment has improved the sensitivity of MoS_2 nanoparticle-anchored LIG-based humidity sensors.[25] Moreover, plasma oxidation has been used to create oxidized LIG with enhanced performance in the oxygen evolution reaction.[26] Additionally, plasma-treated LIG electrodes have been utilized in organic electrochemical transistors (OECT).[27]

While previous studies have demonstrated the benefits of plasma treatment in enhancing the properties of LIG, they did not study the effect of plasma on LIG in detail and they have primarily focused on short treatment durations. As a result, the effect of extended plasma exposure on LIG's structural and

https://doi.org/10.1021/acsanm.5c02542
ACS Appl. Nano Mater. 2025, 8, 17052−17064

electrochemical properties remains unexplored. Since longer treatment durations could enhance performance by further improving surface wettability and chemistry if negative effects can be avoided, a detailed investigation is necessary to assess these effects thoroughly. This research addresses this gap by examining the effects of varying plasma treatment durations on the material characteristics and electrochemical performance of LIG-based sensors. By doing so, we establish an optimal treatment window that enhances electrochemical performance while preventing overexposure that degrades material integrity.

2. MATERIALS AND METHODS

2.1. Materials and Chemical Reagents. Polyimide film (Kapton tape) was purchased from Creative Global Services Limited (Newmarket, Canada) as a substrate for conversion into LIG. Potassium ferricyanide ($K_3[Fe(CN)_6]$); potassium hexa-cyanoferrate-(II) trihydrate ($K_4Fe(CN)_6{\cdot}3H_2O$), and potassium chloride (KCl) were purchased from Sigma-Aldrich (Oakville, Canada) for making the analyte solution for electrochemical testing with our plasma treated LIG electrodes.

2.2. Electrochemical Analyte Selection and Preparation. In this study, we performed electrochemical characterization of the standard potassium ferrocyanide/potassium ferricyanide redox system using a fully integrated LIG based electrochemical sensor. $K_3[Fe(CN)_6]$ and $K_4Fe(CN)_6{\cdot}3H_2O$ are widely used in physiological experiments for their role in modulating cellular redox reactions.[28,29] They were chosen from a variety of popular redox systems for its surface-sensitive electrochemical response, making it particularly suitable for the study of carbon-based materials.[30−32] The analyte solution was prepared in deionized (DI) water, with 0.1 M KCl, and mixed thoroughly using a vortex mixer. A 100 mM stock solution was initially prepared, and lower concentrations down to 0.04 mM were obtained through serial dilution.

2.3. LIG Electrode Fabrication and Plasma Treatment. A LIG-based three-electrode system was designed using manual coding and converted into G-Code for use in the Repetrel software of the Hydra 16 A printer (Hyrel, Norcross) with a 40 W CO_2 laser. Graphene was fabricated by scribing a piece of Kapton tape of 125 μm thickness attached to a glass slide (Figure 1a(i,ii)). To identify the optimal laser settings for minimizing sheet resistance, the laser power was studied and adjusted from 18% to 28% of its maximum 40 W output in 2% increments, while the scan speed spanned from 60 to 360 mm/min with a step size of 60 mm/min. The three LIG electrodes were designed to serve as the reference electrode (RE), working electrode (WE), and counter electrode (CE) in CV and EIS of the above-mentioned standard water samples (see next section).

After the fabrication of the three-electrode LIG system, the device underwent air plasma treatment using a MARCH PLASMOD plasma system (MARCH, Concord USA), in conjunction with a T&C power converter (Figure 1a(iii)). The plasma treatment was conducted at a power level of 25 W, with treatment durations ranging from 10 to 60 s in 10 s increments, as well as an extended interval of 120 s.

2.4. Electrochemical Characterization and Data Analysis. CV measurements were performed using the fabricated three-electrode system immersed in 20 mL of analyte solution in a beaker as shown in Figure 1a(iv). To ensure a consistent and controlled effective working area, we carefully designed the LIG patterning on the polyimide film such that the WE area maintained consistent contact with the analyte solution during each measurement. The wetted surface area was measured multiple times after electrode immersion to confirm reproducibility. This approach allowed us to verify that the exposed WE area remained constant across all tests, thereby minimizing variability and ensuring reliable electrochemical characterization. The experiments were conducted at room temperature with an Autolab potentiostat (Utrecht, Netherlands) controlled by Nova 2.1 software. The potential was swept from −0.8 to 0.8 V at a scan rate of 100 mV/s. This potential window was selected to accurately capture the peak potential across different treatment times and analyte concentrations. While previous studies have typically used a narrower range of −0.3 to 0.5 V for potassium ferrocyanide/ferricyanide analyte solutions,[33] our extended range ensures precise detection of any subtle potential variations induced by treatment changes. Each experiment consisted of three consecutive scans and the average was used for analysis. The anodic and cathodic peak currents for all the CV scans were determined by identifying the maximum (anodic) and minimum (cathodic) currents, where the peaks were observed in the scan plots, ensuring consistency. The difference between anodic and cathodic peak currents was calculated to determine ΔI_p. The LOD was determined based on the standard deviation of measurements from the blank solution and low-concentration samples. For lower analyte concentrations, where no detectable peaks were observed (precisely, 0.04 mM−0.5 mM for untreated devices and 0.04 mM−0.06 mM for plasma-treated devices), the ΔI_p was measured as the difference between the highest and lowest currents within the −0.5 to 0.5 V range. This voltage range was chosen as it encompasses the redox peaks observed at higher concentrations, making it the relevant faradaic region for electrochemical analysis. Additionally, a blank solution of 0.1 M KCl, without the analyte, was analyzed within the same voltage range for both untreated and plasma-treated devices to ensure a consistent comparison. A detailed description of the method to calculate LOD from these results is given in Section 1, Supporting Information. The LOQ is defined as the lowest concentration of the analyte that can be reliably quantified. In this study, the LOQ was determined by multiplying the LOD by a factor of 3.3.[34] Data processing and graph generation were performed using Origin 2024b software.

EIS experiments were accomplished using Autolab potentiostat over a frequency range from 0.1 Hz to 10 kHz, with a potential perturbation amplitude of 1 mV versus the open-circuit potential (OCP). These measurement settings were selected based on literature ref 33, as they provided accurate results with a well-fitted equivalent circuit model, eliminating the need for further adjustments. All experiments were conducted at room temperature to ensure consistency across measurements. Three devices were tested for each plasma treatment condition, and the averaged results were used to generate the Nyquist plot. To determine the EIS parameters—including solution resistance (R_s), R_{ct}, electric double-layer capacitance (C_{dl}), and the Warburg element (W_e)—an equivalent circuit model was fitted to the data from all three devices. The measured values were then averaged, and error bars were calculated based on the standard deviation of these three data sets to represent variations in EIS parameters.

Statistical analysis was performed to evaluate the significance of changes in EIS parameters and LOD across different conditions. A *t* test was conducted to assess whether the observed variations were statistically significant. For each condition, three measurements were taken, and the *p*-values from the *t* test were calculated to quantify the significance of differences between data sets.

2.5. Materials Characterization. *2.5.1. Contact Angle Measurement.* Contact angle measurements were performed using the Krüss FM 40 Easy Drop Contact Angle Measuring System (KRÜSS Scientific, Hamburg, Germany) and Drop Shape Analyzer software. A droplet was dispensed onto the substrate using a syringe pump at a controlled flow rate of 500 μL/min. Images were captured once the droplet stabilized on the surface, ensuring accurate measurements. The acquired images were further processed and analyzed using ImageJ software. To account for surface variability, five measurements were taken at different locations on the LIG surface. The error bars were calculated based on the variation among these five readings.

2.5.2. Sheet Resistance Measurement. The sheet resistance of the inscribed LIG was measured using a four-point probe system (Ossila, Sheffield, UK). For each measurement, 5 mm × 5 mm square samples were prepared. To ensure accuracy, five measurements were taken from each of the five samples for every laser power and speed setting. The calculated error bars, based on measurement variations, were incorporated into the figures.

2.5.3. SEM Analysis. The morphological and structural characterization of the LIG samples was performed using a TESCAN VEGA3

https://doi.org/10.1021/acsanm.5c02542
ACS Appl. Nano Mater. 2025, 8, 17052−17064

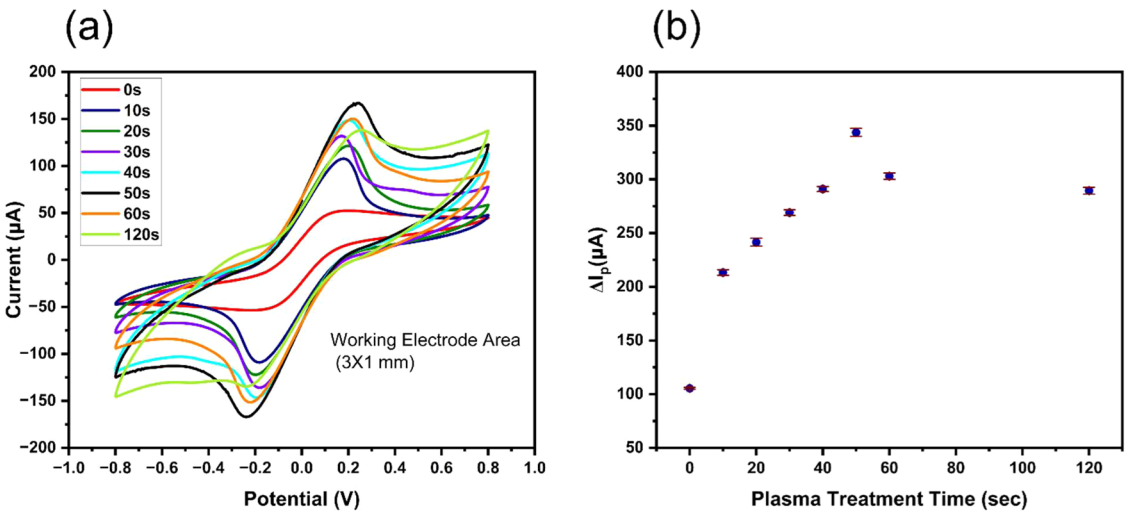

Figure 2. Effect of plasma treatment time on electrochemical performance (a) CV measurements for devices subjected to different plasma treatment durations as shown in the legend. (b) Plot of peak-to-peak current (ΔI_p) as a function of plasma treatment time.

scanning electron microscope (TESCAN, Brno, Czech Republic). High-resolution images were captured to evaluate the quality and surface features of the fabricated LIG.

2.5.4. Raman Spectroscopy. Raman spectra were recorded using a LabRAM ARAMIS Raman Microscope (HORIBA Scientific, Piscataway, USA) with a 532 nm laser excitation and a laser power of 50 mW. The I_D/I_G ratio was determined using Origin software by performing Gaussian peak fitting on the D (~1350 cm^{-1}) and G (~1580 cm^{-1}) peaks after baseline correction. The integrated areas under these fitted peaks were then used to calculate the ratio, with the D-band area divided by the G-band area.

2.5.5. X-ray Photoelectron Spectroscopy (XPS). XPS analysis of the samples was performed using the K-α XPS system (Thermo Fisher Scientific, Massachusetts, USA). Peak fitting of XPS spectra was performed in Origin software using a Gaussian function after baseline correction. The peaks were deconvoluted within the defined binding energy ranges corresponding to specific elements or functional groups. Fitting parameters were optimized to minimize residual error and ensure accuracy.

3. RESULTS

The fabrication process of LIG began with the careful optimization of laser operating power and scan speed to achieve the lowest possible sheet resistance, as detailed in Figure S2 (Supporting Information). Using optimized laser settings of 24% laser power and a laser scan speed of 120 mm/min, a three-electrode system was fabricated for further analysis.

3.1. Effect of Plasma Treatment Time on Cyclic Voltammetry of LIG Based Sensors. To assess the impact of plasma treatment with different exposure times on the sensor's performance of a three-electrode LIG system, both untreated and plasma-treated samples were analyzed using CV at room temperature. For Faradaic testing, a redox probe solution of 5 mM ferricyanide/ferrocyanide was used with 100 mM potassium chloride as the supporting electrolyte. The CV data of the devices treated with different plasma treatment times is shown in Figure 2(a). The *y*-axis represents the WE current in this figure, while the *x*-axis corresponds to the applied potential. The difference between the anodic and cathodic peak currents (ΔI_p) as a function of plasma treatment time is shown in Figure 2(b). The oxidation peaks in all measurements are observed within the potential range of 0.15 to 0.25 V. In comparison, the reduction peaks are detected between −0.1 V and −0.25 V. These values closely correspond to those reported in the literature for this analyte, confirming the consistency of the results.[33]

The results presented in Figure 2(a),2(b) demonstrate that air plasma treatment significantly enhances the performance of the three-electrode LIG system. For instance, the ΔI_p value of the untreated three-electrode system is 105.4 μA which improved markedly to 213.3 μA following 10 s of plasma exposure. The value continues to rise, reaching 343.7 μA at 50 s of plasma treatment. However, a decline in performance was observed with extended plasma exposure, with ΔI_p values decreasing to 303 μA at 60 s and 289.66 μA at 120 s. The improved sensor performance after air plasma treatment is attributed to changes in LIG surface properties, including increased hydrophilicity and electrocatalytic activity. However, overexposure (>50 s) introduces defects that reduce conductivity and sensor performance. The decrease in conductivity is presented in the Supporting Information (Figure S3). The following sections will discuss these trends in detail.

3.2. Cyclic Voltammetry Based Limits of Detection and Quantification Analysis. To determine the LOD and LOQ for both untreated and optimized plasma-treated devices (50 s treatment), CV scans were conducted at varying analyte concentrations to generate a dose−response curve for each device. A detailed explanation about how the LOD and LOQ was determined is provided in Supporting Information (see SI Section 1). Figure 3(a),3(b) show the CV data for all analyte concentrations under untreated and plasma-treated conditions. To provide a clearer view of the variations at lower concentrations, Figure 3(c),(d) show a zoomed-in analysis focusing on the 0.04 mM−1 mM range. Figure 3(e) illustrates the dose−response curves of the two devices and the variation in peak-to-peak current across these conditions.

The analysis shows that detectable anodic and cathodic peaks for untreated devices appear at a minimum concentration of 1 mM, with lower concentrations failing to produce distinguishable signals. As a result, ΔI_p values are similar at lower concentrations to those of the blank solution. However, from 1 mM onward, a linear increase in current is observed with rising concentration. In contrast, plasma-treated devices (treated for 50 s) exhibit detectable peaks at concentrations as

https://doi.org/10.1021/acsanm.5c02542
ACS Appl. Nano Mater. 2025, 8, 17052−17064

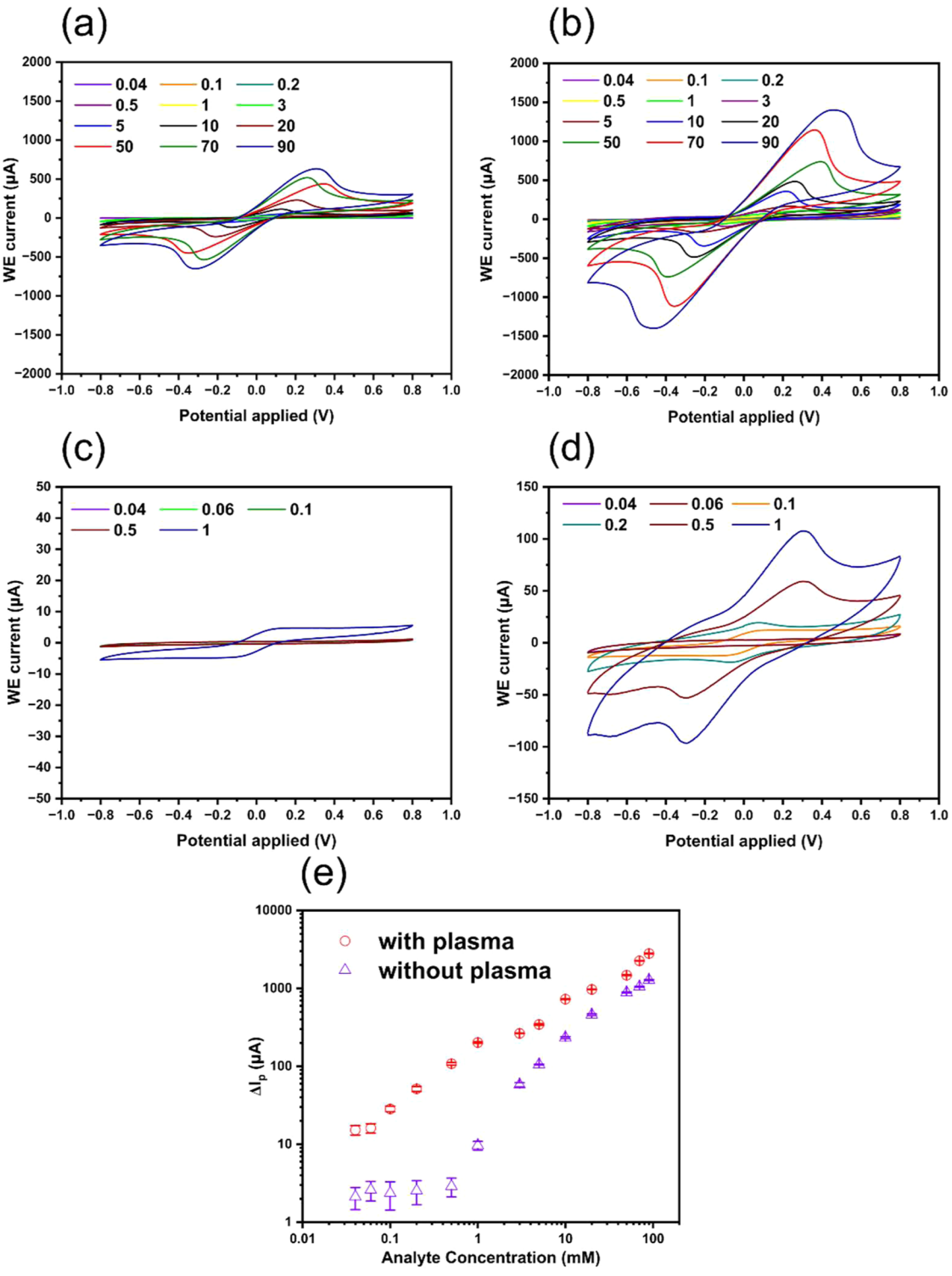

Figure 3. CV responses for varying analyte concentrations (legends in mM) in (a) untreated devices and (b) devices subjected to a 50 s oxygen plasma treatment. To examine peak current at lower analyte concentrations (0.04 mM−1 mM), CV results are presented for (c) untreated and (d) plasma-treated devices. (e) Plot of ΔI_p as a function of analyte concentration. At high concentrations, ΔI_p increases monotonically with concentration. At very low concentrations, ΔI_p is not a function of concentration and no detectable peaks were observed. The concentration at which the peak becomes distinguishable from the blank solution transitioning between regimes is higher for untreated electrodes.

low as 100 μM, followed by a linear increase in current with increasing concentration. The transition between no clear and distinguishable peaks from the blank solution happens at a higher concentration for untreated electrodes, which means a clear shift in the performance between the untreated and plasma-treated electrodes. Based on this observation, the LOD for the treated devices was calculated to be 70 μM, whereas for the untreated devices, it was 927 μM. The LOQ was determined to be 230 μM for the treated devices and 3.06 mM for the untreated devices. This significant enhancement

https://doi.org/10.1021/acsanm.5c02542
ACS Appl. Nano Mater. 2025, 8, 17052−17064

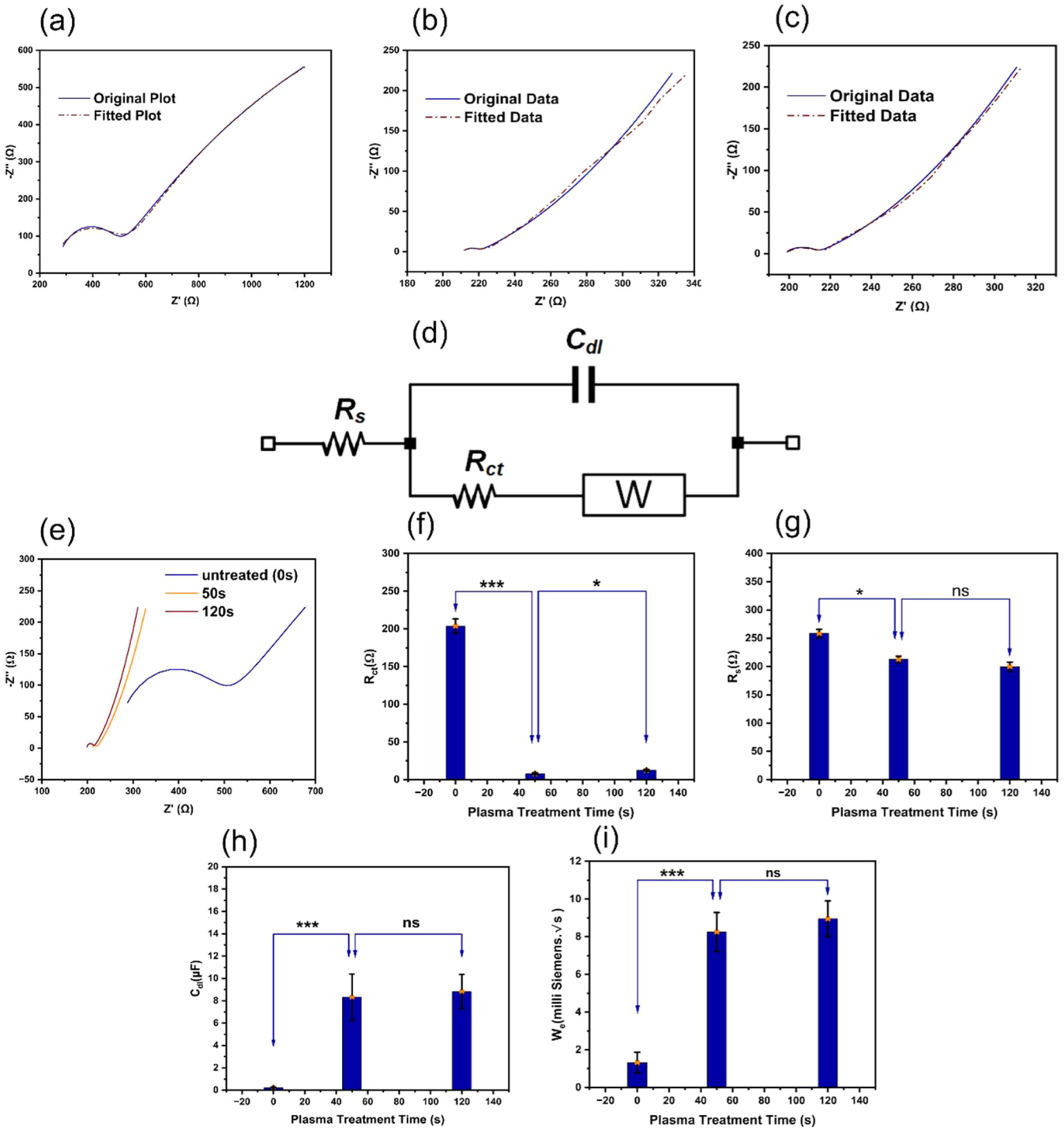

Figure 4. EIS analysis of LIG electrodes. (a–c) Nyquist plots showing the impedance response of electrodes with different plasma treatment times: (a) untreated, (b) 50 s plasma-treated, and (c) 120 s plasma-treated. (d) The equivalent circuit model is used for calculating R_s, R_{ct}, C_{dl}, and W_e. (e) Comparative analysis of the impedance data for all three conditions. (f–i) Quantitative analysis of extracted electrochemical parameters with statistical significance (p-values): (f) R_{ct} decreases significantly from 0 to 50 s (p = 0.00015) but increases at 120 s (p = 0.014). (g) R_s shows a moderate decrease from 0 to 50 s (p = 0.016) but remains largely unchanged from 50 to 120 s (p = 0.073). (h) C_{dl} increases significantly from 0 to 50 s (p = 0.000726) but stabilizes between 50 and 120 s (p = 0.41). (i) W_e follow a similar trend, with a significant increase from 0 to 50 s (p = 0.00013) but no substantial change beyond 50 s (p = 0.14). Statistical significance is denoted as follows: $p < 0.05$ (*), $p < 0.01$ (**), and $p < 0.001$ (***).

highlights the role of plasma treatment in improving device sensitivity.

3.3. Electrochemical Impedance Spectroscopy Analysis. To investigate the impact of different plasma exposure times on the properties of the electrode–electrolyte interface, EIS was conducted on the fabricated devices with three different plasma treatment conditions: untreated, optimized treatment (50 s, as determined in the previous section), and extended treatment (120 s) to assess the effects of overexposure. The Nyquist plots of the impedance for the three

https://doi.org/10.1021/acsanm.5c02542
ACS Appl. Nano Mater. 2025, 8, 17052–17064

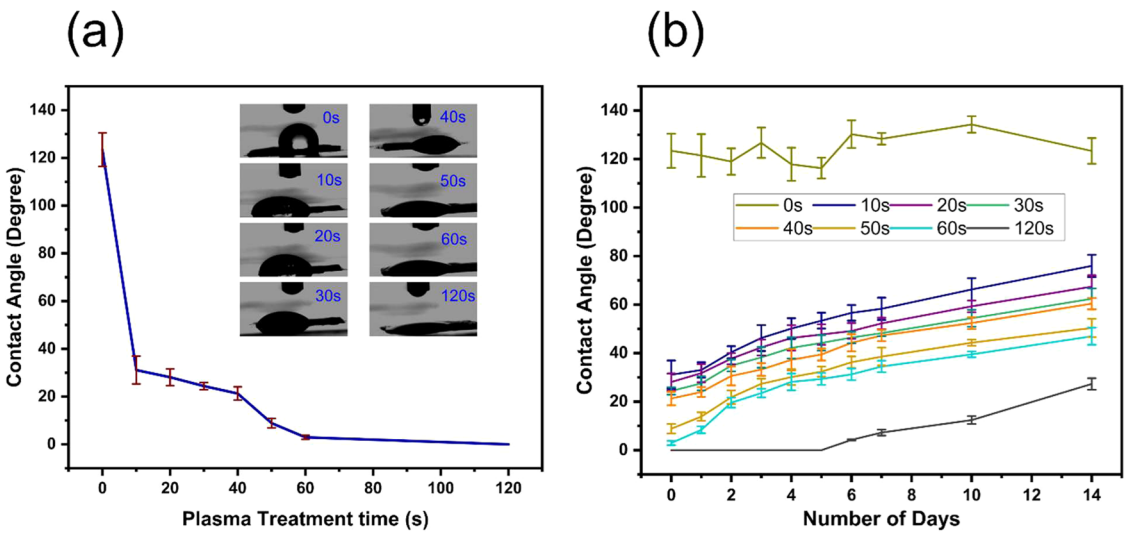

Figure 5. Effect of plasma treatment on wettability and its long-term stability. (a) Influence of plasma treatment duration on the wettability of LIG surfaces, measured by the contact angle of a DI water droplet. Inset images show droplet behavior on each surface, illustrating the changes in wettability. (b) Long-term stability of wettability over 14 days for LIG surfaces with different plasma treatment durations.

plasma conditions are shown in Figure 4(a–c), along with the fitted line based on the equivalent circuit model shown in Figure 4(d). Figure 4(e) shows a comparison of all three conditions. A comparison of the R_s, R_{ct}, C_{dl}, and W_e is presented in Figure 4(e–h) with the result of a t test showing the significance of the difference between the conditions.

The data indicate that plasma treatment significantly reduces R_{ct}, which represents the resistance ions encounter when moving from the electrolyte to the electrode during a reaction.[35] Plasma treatment introduces oxygen-containing functional groups onto the electrode surface, significantly improving its affinity for the electrolyte. This enhanced electrode–electrolyte interaction facilitates more efficient charge transfer, leading to a marked reduction in R_{ct} (Figure 4(f)). For instance, the device treated for 50 s shows a R_{ct} of 7.86 ± 1.12 Ω, a significant decrease compared to the untreated sample, which has a R_{ct} of 203.65 ± 9.56 Ω. However, prolonged plasma exposure (120 s) increases R_{ct}, reaching 12.4 ± 0.85 Ω. This rise in R_{ct} highlights that while plasma treatment enhances electrochemical performance at 50 s, excessive exposure (120 s) leads to an increase in R_{ct}, reducing charge transfer efficiency. It is likely due to the disruption of the conductive network at the surface of the electrode, which is caused by an overabundance of defects on the surface. These defects negatively impact the electrode–electrolyte interaction, reducing charge transfer efficiency.[36] The 50 s treatment duration provides optimal performance, as also evidenced by the improved CV results in Figure 2.

As plasma treatment duration increases, the R_s decreases (Figure 4(g)). Precisely, R_s is measured at 258.7 ± 7.45 Ω for the untreated sample, reducing to 212.6 ± 5.96 Ω after 50 s of plasma treatment. A further decline to 199.2 ± 8.12 Ω is observed following 120 s of treatment, indicating a progressive reduction in R_s with extended plasma exposure. This reduction in R_s can be attributed to the enhanced wettability of the porous electrode, which allows more liquid electrolyte to penetrate it, thus lowering its electrical resistance. As the treatment time increases, the plasma effectively removes contaminants and residues from the electrode surface, resulting in a cleaner, more accessible surface. This improved surface integrity allows ions to approach the electrode more easily, enhancing ionic conduction.

At the interface of the electrode and electrolyte, an electric double layer is formed, which is represented as a capacitor.[37] Therefore, an increase in the electrode's active surface area enhances the capacitance of this double layer. Plasma treatment of the electrode surface significantly increases its active area, promoting greater interaction between the electrode and the analyte. As a result, the capacitance of the plasma-treated electrodes is substantially higher (Figure 4(h)). Specifically, for electrodes treated for 50 and 120 s, the C_{dl} values are 8.33 ± 2.07 μF and 8.82 ± 1.53 μF, respectively, compared to the much lower capacitance of the untreated devices, which is 0.235 ± 0.04 μF. This increase in capacitance highlights the improved electrode-analyte interaction enabled by plasma treatment, enhancing the overall electrochemical performance.

The W_e values (Figure 4(i)) for plasma-treated devices are significantly higher than those of the untreated devices, which exhibit a value of 1.32 ± 0.56 $mS{\cdot}s^{0.5}$. There is no substantial difference between the plasma-treated devices, with W_e values of 8.25 ± 1.03 $mS{\cdot}s^{0.5}$ for the 50 s treatment and 8.95 ± 0.95 $mS{\cdot}s^{0.5}$ for the 120 s treatment. These results indicate that plasma exposure enhances analyte diffusion at the electrode surface, which is markedly weaker in the untreated devices.

3.4. Effect of Plasma Treatment on the Contact Angle of LIG Surface over Time. To understand the impact of plasma treatment duration on electrochemical performance, we conducted physical characterization of LIG, beginning with wettability analysis. To investigate the change in wettability as a function of plasma treatment duration, contact angle of deionized water on LIG samples subjected to varying plasma treatment durations was measured and is shown in Figure 5(a). The inset images illustrate the variation in contact angle on the LIG samples, corresponding to different plasma treatment durations. The treatment times range from no plasma treatment up to 120 s, with a constant power setting of 25 W. The data shows that the contact angle decreases with increasing plasma treatment time. Initially, without plasma treatment, the contact angle was 123.4° ± 7.04°. After just 10 s

https://doi.org/10.1021/acsanm.5c02542
ACS Appl. Nano Mater. 2025, 8, 17052–17064

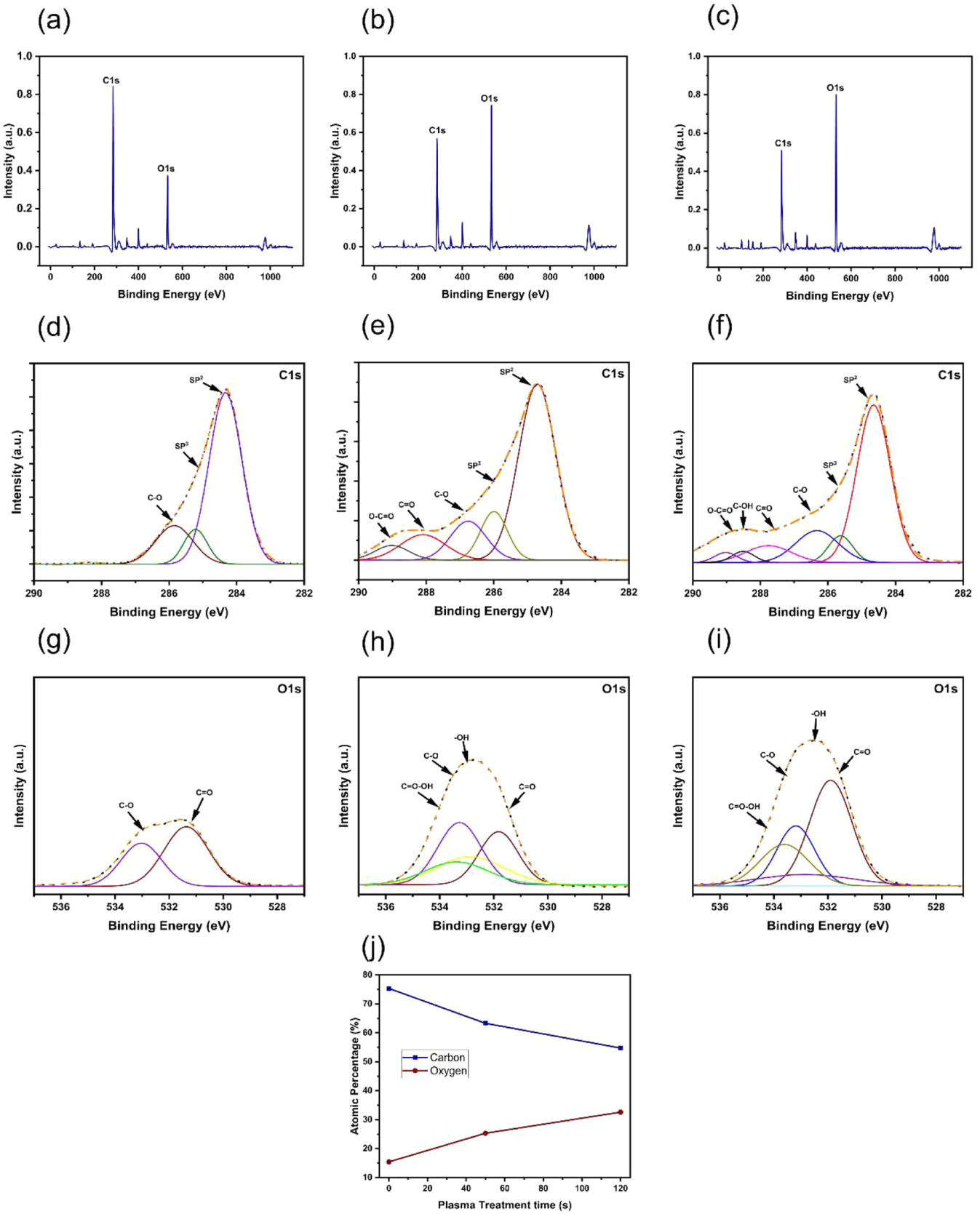

Figure 6. XPS survey spectra for LIG samples at varying plasma treatment durations: (a) untreated, (b) 50 s treated, and (c) 120 s treated. Detailed C 1s spectra for (d) untreated, (e) 50 s treated, and (f) 120 s treated samples, alongside O 1s spectra for (g) untreated, (h) 50 s treated, and (i) 120 s treated LIG, illustrating changes in surface chemistry with increasing treatment time. (j) Atomic percentages of carbon and oxygen as a function of plasma treatment duration, showing increasing oxygen and decreasing carbon content with increasing exposure time.

https://doi.org/10.1021/acsanm.5c02542
ACS Appl. Nano Mater. 2025, 8, 17052−17064

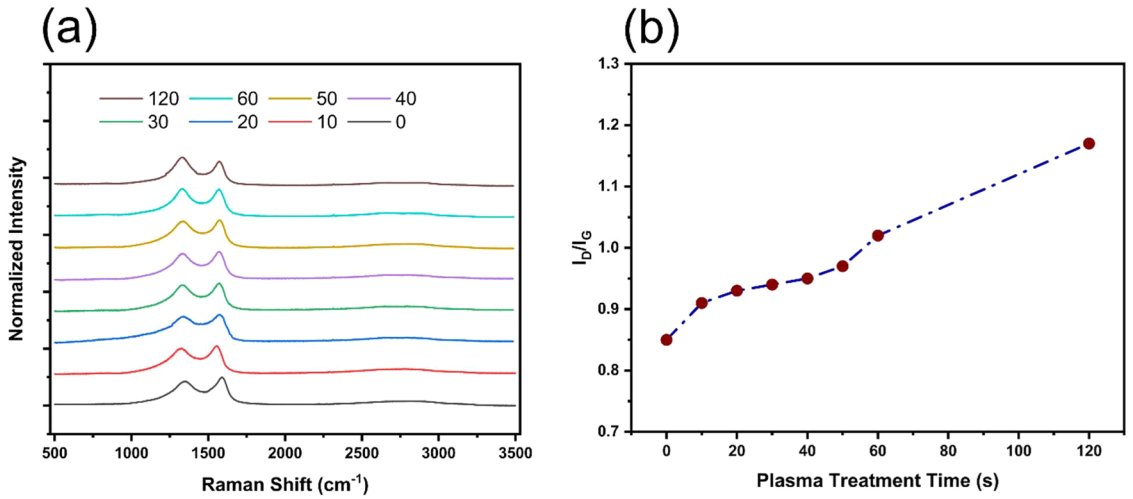

Figure 7. (a) Raman spectroscopy analysis of LIG samples subjected to varying plasma treatment durations. (b) I_D/I_G ratio as a function of plasma treatment duration shows a rise in the ratio, corresponding to an increasing defect density with longer exposure times, ultimately affecting the overall quality of graphene.

of treatment, it drops to 31.2° ± 5.81°, representing a reduction of approximately 75%. As the treatment time increases, the contact angle decreases progressively, reaching 0° at 120 s of plasma exposure. The observed variations can be explained by changes in the amount of oxygen containing chemical groups on the surface of the LIG samples, which will be examined in detail in the following section. Figure 5(b) illustrates the effect of plasma treatment duration on LIG samples over a 14-day storage period under ambient conditions.

The data show that while the contact angle remains constant for the untreated sample, it gradually increases over time for all plasma-treated samples, indicating a decrease in wettability. However, the effect of plasma treatment persists even after 14 days, as none of the treated surfaces return to the contact angle of the untreated sample.

Specifically, the sample treated for 10 s exhibited a contact angle increase of approximately 45° over 14 days, reaching 76°, suggesting that it remained hydrophilic. Similarly, the 50 s treated sample showed an increase of 41°, with a final contact angle of 50.37°, while the 120 s treated sample exhibited a smaller increase of 27°. These findings demonstrate that although wettability gradually decreases over time, plasma treatment still effectively enhances surface hydrophilicity, with its influence remaining evident even after 2 weeks.

These results indicate that increasing plasma treatment duration enhances surface wettability and consequently electrochemical performance. However, the underlying reason why excessive exposure negatively impacts electrochemical performance remains unclear. Further investigation, presented in the following sections, explores additional factors influencing this phenomenon.

3.5. X-ray Photoelectron Spectroscopy (XPS) Analysis. To examine the reason behind the effect of plasma treatment duration on the wettability of LIG samples, XPS analysis was conducted on three sample groups: untreated (0 s), 50 s plasma-treated, and 120 s plasma-treated. Figure 6(a–c) presents the elemental composition of the surface. The data indicate a progressive increase in oxygen concentration on the surface of the LIG samples with extended plasma treatment time, accompanied by a corresponding decrease in carbon concentration. This trend is quantitatively represented in the atomic concentration plot in Figure 6(j), where the carbon content is shown to decrease from 75.4% in untreated samples to 64.4% and 54.7% after 50 and 120 s of plasma exposure, respectively.

Conversely, oxygen concentration of the untreated sample is 15.8% which is found higher as 25.4% and 32.6% for 50 and 120 s plasma treated samples, respectively. The C 1s spectrum, presented in Figure 6(d–f) was deconvoluted into distinct peaks corresponding to different chemical states, based on their individual binding energies: sp^2-hybridized carbon (C═C, 284.5 eV), carbon oxygen single bond (C–O, 285.9 eV), carbonyl group (C═O, 288.2 eV), carboxyl group (O–C═O, 289.1 eV), and aldehyde group (–CHO, 288.4 eV).[38] The results indicate that the 120 s plasma-treated sample shows a prominent presence of all the peaks mentioned, including C–O, C═O, and O–C═O and CHO. However, in the 50 s treated sample, the presence of all the functional groups was found but their intensity was less compared to the 120 s plasma treated sample. These findings show that as the treatment time increased, the intensity of polar oxygen functional groups increased. As a result, the interaction of water with the surface was much stronger, causing the increase in the wettability of the surface as observed in Figure 5.[20] The O 1s spectra also contain C–O (≈533.5 eV) and C═O (≈531.9 eV) groups as presented in Figure 6(g),6(h),6(i).[26] The findings highlight the influence of plasma treatment duration on the peak intensity of oxygen-containing surface groups in LIG samples. Functional groups such as C═O and C–O forming on the LIG surface during plasma exposure are critical in enhancing wettability. Increased wettability, in turn, improves the interaction between the electrolyte and the electrode surface, facilitating more effective electrochemical performance.[21] These surface groups may also create active sites that facilitate the interaction of electroactive atoms. Consequently, as plasma treatment time increases, the number of active sites and the wettability of the LIG surface are enhanced, leading to improved electrochemical reactivity and overall performance.

3.6. Physical Characterization (Raman Spectroscopy) of the LIG Samples. Raman spectroscopy was conducted to

https://doi.org/10.1021/acsanm.5c02542
ACS Appl. Nano Mater. 2025, 8, 17052–17064

evaluate the quality of LIG and to understand the factors influencing the performance of the LIG-based sensor. This analysis aimed to identify the reasons behind the initial increase in sensor performance and the subsequent decrease observed after a specific time limit. It is a widely utilized nondestructive technique that identifies structural defects within carbon-based materials like LIG. Raman spectra of the LIG samples with different plasma treatment times are depicted in Figure 7(a). The SEM images of these LIG surfaces are shown in Figure S4 (Supporting Information).

The Raman spectrum of the untreated (0 s) LIG material reveals the presence of distinct peaks positioned around 1349.6 cm^{-1} and 1587.9 cm^{-1}, representative of the D and G bands, respectively. Correspondingly, the oxygen plasma-treated LIG materials with different treatment times exhibit symmetrical representative peaks within the identical spectral region. The G band in the Raman spectrum, typically observed around 1580 cm^{-1}, is attributed to the in-plane vibrations of sp^2-bonded carbon atoms within the graphene lattice. Conversely, the D band, located near 1350 cm^{-1}, signifies structural defects, disorder, and the presence of sp^3-hybridized carbon atoms in the graphene structure.[39,40]

The intensity ratios of D and G peaks (I_D/I_G) for LIG with different exposure times to oxygen plasma treatment is shown in Figure 7(b). The I_D/I_G ratio in the Raman spectra is a key indicator of the quality and structural properties of graphene, serving as an indication of heightened disorder within the structure as the oxygen plasma-treatment time increases. A higher ratio indicates more defects in the graphene structure. Defects can increase the density of active sites, and internal roughness within the material, which might enhance electron transfer.[41]

An excessive number of defects can disrupt the conductive network, leading to a small increase in sheet resistance (as shown in Figure S3, Supporting Information), while compromising the material's quality by introducing a higher density of structural irregularities. These defects can reduce the CV current due to increased R_{ct}. Defects can act as catalytic sites that facilitate electron transfer, enhancing the peak current for redox probes.[21] However, if the defect density is too high, it can create barriers to electron flow and reduce the peak current. Furthermore, while increased defect density may enhance surface roughness and the graphene electrode's effective surface area, potentially improving sensor performance, this effect is beneficial only up to an optimal threshold. Beyond this point, the excessive introduction of defects negatively impacts conductivity and electrochemical behavior.

3.7. Durability and Stability of Plasma-Treated Sensors. To assess the durability of the sensors after plasma treatment, their performance was evaluated over a 90 days period using the same CV setup. Two devices from each group were tested daily, and the average difference between anodic and cathodic peak currents was calculated and normalized against the Day 0 value. As shown in Figure 8, the performance of both sensor groups remained stable throughout the 14-day period. After 90 days of storage under ambient conditions, both untreated and plasma-treated sensors exhibited only a ~20% decrease in performance, indicating excellent durability and minimal degradation over time.

The small reduction in performance over time may be due to partial deactivation of plasma-generated active sites and the adsorption of airborne contaminants, which can affect the integrity of the conductive network.[42] However, this similar trend in both groups suggests that the decline is not primarily attributable to plasma treatment. While some loss of surface functional groups likely occurred, it did not substantially compromise sensor performance. Overall, the sensors demonstrated robust and consistent performance under real-world storage conditions.

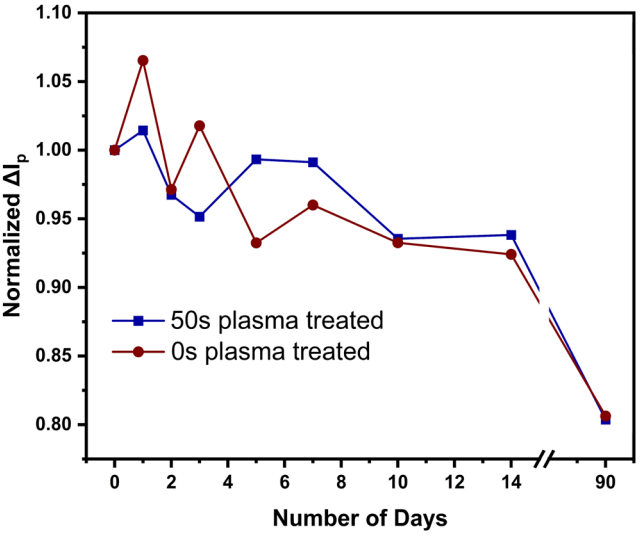

Figure 8. Comparative analysis of CV peak to peak currents (normalized against day 0) for untreated and 50 s plasma-treated sensors, recorded daily over a 14-day period and on day 90. Both untreated and 50 s plasma-treated sensors exhibit consistent electrochemical performance, indicating stability and reliability over time.

4. DISCUSSION

The impact of plasma treatment duration on the performance of LIG-based electrochemical sensors reveals a key balance between beneficial surface modifications and excessive structural changes. The observed trends in CV and EIS indicate that moderate plasma exposure enhances sensor performance, whereas prolonged treatment introduces adverse effects.

The initial increase in anodic and cathodic peak currents with plasma treatment up to 50 s can be attributed to improved wettability introducing oxygen-containing functional groups, as confirmed by XPS and increased defect density on the LIG surface. Contact angle measurements demonstrated a significant reduction in water contact angle with increasing plasma exposure, indicating enhanced hydrophilicity.[26] Plasma treatment introduces a range of oxygen-containing surface functional groups, including −OH, C═O, and −COOH, which significantly influence the electrode−electrolyte interface. These groups increase the surface polarity and improve wettability, allowing better diffusion of the electrolyte and more effective interaction with electroactive species.[43] In the case of the $[Fe(CN)_6]^{3-/4-}$ redox system used in this study, these functionalities can promote stronger electrostatic and hydrogen-bonding interactions, enhancing the adsorption and electron transfer between the redox couple and the electrode surface.[44] The reduction in R_s and R_{ct} observed in EIS further supports this, indicating an improvement in ionic conductivity and charge transfer efficiency. Additionally, the increase in electric double-layer capacitance and the reduction in the Warburg impedance suggest more efficient ion diffusion and

https://doi.org/10.1021/acsanm.5c02542
ACS Appl. Nano Mater. 2025, 8, 17052−17064

enhanced interfacial charge transfer, which is crucial for optimal sensor performance.[33]

Raman spectroscopy revealed a rise in the I_D/I_G ratio, confirming that plasma treatment introduces additional structural defects, which act as active sites and can enhance charge transfer.[41] This facilitates more effective electrolyte penetration into the porous graphene network, thereby improving ion transport and increasing the accessibility of electroactive sites. However, it is important to note that excessive plasma exposure such as at 120 s leads to a further increase in defect density, which may begin to disrupt the conductive graphitic network of the LIG. This overoxidation or overfragmentation can degrade electrical conductivity and reduce the overall efficiency of electron transfer pathways. As a result, excessive plasma treatment led to a decline in electrochemical performance, as the increase in R_{ct} by approximately 20% suggests that excessive surface modification may introduce defects that hinder electron mobility.[41] While a moderate level of defect density can enhance ionic conductivity by providing more active sites, an excessive number of defects may disrupt the overall conductive network, ultimately leading to a decline in electrode performance.[36] The balance between functionalization and structural integrity is thus a key determinant in optimizing plasma treatment duration.

An important performance indicator of electrochemical sensors is their LOD. Our results demonstrate a 10-fold improvement in LOD and LOQ for the 50 s plasma-treated sensor compared to the untreated sensor. This substantial enhancement underscores the effectiveness of plasma treatment in increasing the sensitivity of LIG-based sensors. The durability tests further confirm the stability of both untreated and treated sensors over 14 days, reinforcing the reliability of these sensors for prolonged use.

5. CONCLUSIONS

In conclusion, this study demonstrates the significant impact of plasma treatment time, at a specific power level, on performance of LIG-based electrochemical sensors using a well-established $Fe(CN)_6^{3-/4-}$ redox couple. Our findings reveal that plasma treatment enhances sensor performance only up to an optimal threshold time, beyond which further treatment time leads to decreased performance compared to the optimal point. At 25 W plasma power, a treatment duration of 50 s resulted in a 243% increase in peak current, significantly improving CV response. However, exceeding this duration did not improve the sensor's performance; instead, compared to 50 s, it decreased. This trend can be attributed to increased wettability and defect formation due to plasma exposure. While enhanced wettability generally improves electrochemical interactions, excessive defects beyond a specific treatment duration disrupt charge transfer, despite wettability reaching its maximum. Defect formation becomes the dominant factor, emphasizing that wettability alone is insufficient for effective electrochemical performance. These results emphasize the need for precise control of plasma treatment parameters to maximize the electrochemical efficiency of LIG-based sensors and avoid detrimental overprocessing effects. Based on the results from CV and EIS, 50 s was identified as the optimal plasma treatment duration. Although EIS measurements were not conducted at 60 s, the CV data clearly showed a decline in current at 60 and 120 s, while EIS results at 120 s revealed an increase in R_{ct}, confirming the detrimental effect of overexposure.

All three sensor electrodes were fabricated without additional modifications through direct laser scribing on a Kapton tape. This approach significantly simplifies the fabrication process compared to traditional methods, making it both cost-effective and scalable for large-scale production. Such a method holds immense potential for developing affordable, high-performance sensors. Additionally, the durability testing of the sensors provides valuable insights into their long-term stability and reliability, highlighting the practical viability of this fabrication approach for real-world sensing applications. Although a slight decrease in performance was observed after 90 days of ambient storage, a similar trend was noted in both the plasma-treated and untreated sensors, indicating that the decline is not solely due to the plasma treatment. To further preserve surface hydrophilicity and minimize performance degradation over time, storing the sensors in a vacuum or desiccator is recommended as an effective strategy to prevent contamination and maintain long-term functionality. While this study demonstrates lab-scale optimization, future efforts should explore scalable plasma treatment strategies, such as roll-to-roll processing, to enable industrial applications while addressing challenges like uniformity, throughput, and cost. Although this study focused on a single redox probe, future investigations will explore additional redox systems to further assess the versatility, stability, and application-specific performance of plasma-treated LIG electrodes.

■ ASSOCIATED CONTENT

Supporting Information

The Supporting Information is available free of charge at https://pubs.acs.org/doi/10.1021/acsanm.5c02542.

LOD calculation details, laser parameter optimization data, sheet resistance variation of LIG with plasma treatment time, SEM analysis of LIG under varying plasma treatment durations, SEM analysis of LIG under varying plasma treatment durations with higher magnification to see the subtle differences more prominently, CV analysis for lithium detection using untreated and plasma-treated bare LIG electrodes in LiCl solution (PDF)

■ AUTHOR INFORMATION

Corresponding Authors

Pouya Rezai − *Department of Mechanical Engineering, Lassonde School of Engineering, York University, Toronto, Ontario M3J 1P3, Canada;* orcid.org/0000-0002-5031-8063; Email: prezai@yorku.ca

Gerd Grau − *Department of Electrical Engineering and Computer Science, Lassonde School of Engineering, York University, Toronto, Ontario M3J 1P3, Canada;* orcid.org/0000-0001-5729-9160; Email: grau@yorku.ca

Authors

Saumik Dey Shovan − *Department of Electrical Engineering and Computer Science, Lassonde School of Engineering, York University, Toronto, Ontario M3J 1P3, Canada;* orcid.org/0009-0007-3240-1991

Shapour Jafargholinejad − *Department of Mechanical Engineering, Lassonde School of Engineering, York University, Toronto, Ontario M3J 1P3, Canada*

https://doi.org/10.1021/acsanm.5c02542
ACS Appl. Nano Mater. 2025, 8, 17052−17064

Mohamad Kannan Idris − *Department of Electrical Engineering and Computer Science, Lassonde School of Engineering, York University, Toronto, Ontario M3J 1P3, Canada;* orcid.org/0000-0002-8210-5484

Carlos Rodríguez Perales − *Department of Electrical Engineering and Computer Science, Lassonde School of Engineering, York University, Toronto, Ontario M3J 1P3, Canada; Academic Unit of Electrical Engineering, Autonomous University of Zacatecas, Zacatecas 98000, Mexico*

Aamir Minhas-Khan − *Department of Electrical Engineering and Computer Science, Lassonde School of Engineering, York University, Toronto, Ontario M3J 1P3, Canada*

Complete contact information is available at: https://pubs.acs.org/10.1021/acsanm.5c02542

Notes

The authors declare no competing financial interest.

■ ACKNOWLEDGMENTS

We acknowledge the support of the Natural Sciences and Engineering Research Council of Canada (NSERC), funding reference number CREATE 565163-2022. We also acknowledge the support of the York University Catalyzing Interdisciplinary Research Cluster for Detection and Remediation of Water Contaminants (CIRC-DRWC).

■ REFERENCES

(1) Gibi, C.; Liu, C.-H.; Barton, S. C.; Anandan, S.; Wu, J. J. Carbon Materials for Electrochemical Sensing Application − A Mini Review. *J. Taiwan Inst. Chem. Eng.* **2024**, *154*, No. 105071.

(2) Tajik, S.; Beitollahi, H.; Mohammadi, S. Z.; Azimzadeh, M.; Zhang, K.; Le, Q. V.; Yamauchi, Y.; Jang, H. W.; Shokouhimehr, M. Recent Developments in Electrochemical Sensors for Detecting Hydrazine with Different Modified Electrodes. *RSC Adv.* **2020**, *10* (51), 30481−30498.

(3) Nayak, P.; Kurra, N.; Xia, C.; Alshareef, H. N. Highly Efficient Laser Scribed Graphene Electrodes for On-Chip Electrochemical Sensing Applications. *Adv. Electron. Mater.* **2016**, *2* (10), No. 1600185.

(4) Jampasa, S.; Siangproh, W.; Duangmal, K.; Chailapakul, O. Electrochemically Reduced Graphene Oxide-Modified Screen-Printed Carbon Electrodes for a Simple and Highly Sensitive Electrochemical Detection of Synthetic Colorants in Beverages. *Talanta* **2016**, *160*, 113−124.

(5) Bukkitgar, S. D.; Shetti, N. P.; Kulkarni, R. M.; Nandibewoor, S. T. Electro-Sensing Base for Mefenamic Acid on a 5% Barium-Doped Zinc Oxide Nanoparticle Modified Electrode and Its Analytical Application. *RSC Adv.* **2015**, *5* (127), 104891−104899.

(6) Zhang, T.; Jin, H.; Fang, Y.; Guan, J.; Ma, S.; Pan, Y.; Zhang, M.; Zhu, H.; Liu, X.; Du, M. Detection of Trace Cd2+, Pb2+ and Cu2+ Ions via Porous Activated Carbon Supported Palladium Nanoparticles Modified Electrodes Using SWASV. *Mater. Chem. Phys.* **2019**, *225*, 433−442.

(7) Tian, F.; Li, H.; Li, M.; Li, C.; Lei, Y.; Yang, B. Synthesis of One-Dimensional Poly(3,4-Ethylenedioxythiophene)-Graphene Composites for the Simultaneous Detection of Hydroquinone, Catechol, Resorcinol, and Nitrite. *Synth. Met.* **2017**, *226*, 148−156.

(8) Fenzl, C.; Nayak, P.; Hirsch, T.; Wolfbeis, O. S.; Alshareef, H. N.; Baeumner, A. J. Laser-Scribed Graphene Electrodes for Aptamer-Based Biosensing. *ACS Sens.* **2017**, *2* (5), 616−620.

(9) Bauer, M.; Wunderlich, L.; Weinzierl, F.; Lei, Y.; Duerkop, A.; Alshareef, H. N.; Baeumner, A. J. Electrochemical Multi-Analyte Point-of-Care Perspiration Sensors Using on-Chip Three-Dimensional Graphene Electrodes. *Anal. Bioanal. Chem.* **2021**, *413* (3), 763−777.

(10) Minhas-Khan, A.; Nambi, S.; Grau, G. Low-Resistance Laser-Induced Graphitic Carbon by Maximizing Energy Delivery and Pulse Overlap. *Carbon* **2021**, *181*, 310−322.

(11) Wagh, M. D.; Sahoo, S. K.; Goel, S. Laser-Induced Graphene Ablated Polymeric Microfluidic Device with Interdigital Electrodes for Taste Sensing Application. *Sens. Actuators, A* **2022**, *333*, No. 113301.

(12) Liang, G.; He, Z.; Zhen, J.; Tian, H.; Ai, L.; Pan, L.; Gong, W. Development of the Screen-Printed Electrodes: A Mini Review on the Application for Pesticide Detection. *Environ. Technol. Innovation* **2022**, *28*, No. 102922.

(13) Omastová, M.; Pavlinec, J.; Pionteck, J.; Simon, F.; Košina, S. Chemical Preparation and Characterization of Conductive Poly-(Methyl Methacrylate)/Polypyrrole Composites. *Polymer* **1998**, *39* (25), 6559−6566.

(14) de Oliveira, T. R.; Fonseca, W. T.; de Oliveira Setti, G.; Faria, R. C. Fast and Flexible Strategy to Produce Electrochemical Paper-Based Analytical Devices Using a Craft Cutter Printer to Create Wax Barrier and Screen-Printed Electrodes. *Talanta* **2019**, *195*, 480−489.

(15) Park, C.; Rhyu, H.; Jo, S.; Kang, M. H.; Kang, Y. C.; Song, W.; Lee, S. S.; Lim, J.; Myung, S. Electrochemical Sensor Based on Laser-Induced Graphene and CeO2 for Sensitive and Selective Dopamine Detection. *J. Electroanal. Chem.* **2025**, *977*, No. 118865.

(16) Shokurov, A. V.; Menon, C. Laser-Induced Graphene Electrodes for Electrochemistry Education and Research. *J. Chem. Educ.* **2023**, *100* (6), 2411−2417.

(17) Ameku, W. A.; Negahdary, M.; Lima, I. S.; Santos, B. G.; Oliveira, T. G.; Paixão, T. R. L. C.; Angnes, L. Laser-Scribed Graphene-Based Electrochemical Sensors: A Review. *Chemosensors* **2022**, *10* (12), No. 505.

(18) Dallinger, A.; Steinwender, F.; Gritzner, M.; Greco, F. Different Roles of Surface Chemistry and Roughness of Laser-Induced Graphene: Implications for Tunable Wettability. *ACS Appl. Nano Mater.* **2023**, *6* (18), 16201−16211.

(19) Zhang, Z.; Wilson, J. L.; Kitt, B. R.; Flaherty, D. W. Effects of Oxygen Plasma Treatments on Surface Functional Groups and Shear Strength of Carbon Fiber Composites. *ACS Appl. Polym. Mater.* **2021**, *3* (2), 986−995.

(20) Chytrosz-Wrobel, P.; Golda-Cepa, M.; Stodolak-Zych, E.; Rysz, J.; Kotarba, A. Effect of Oxygen Plasma-Treatment on Surface Functional Groups, Wettability, and Nanotopography Features of Medically Relevant Polymers with Various Crystallinities. *Appl. Surf. Sci. Adv.* **2023**, *18*, No. 100497.

(21) Lu, X.; Yim, W.-L.; Suryanto, B. H. R.; Zhao, C. Electrocatalytic Oxygen Evolution at Surface-Oxidized Multiwall Carbon Nanotubes. *J. Am. Chem. Soc.* **2015**, *137* (8), 2901−2907.

(22) Lee, H.; Ohsawa, I.; Takahashi, J. Effect of Plasma Surface Treatment of Recycled Carbon Fiber on Carbon Fiber-Reinforced Plastics (CFRP) Interfacial Properties. *Appl. Surf. Sci.* **2015**, *328*, 241−246.

(23) Schmidt, H. G. Safe Piranhas: A Review of Methods and Protocols. *ACS Chem. Health Saf.* **2022**, *29* (1), 54−61.

(24) Lv, Y.; Yang, N.; You, M.; Hao, J.; Li, J.; Zhang, M. Treatment Rather than Pretreatment: Electrochemical Activation of Electrodes for Electroanalysis. *Microchem. J.* **2025**, *215*, No. 114422.

(25) Li, C.; Xiong, J.; Zhao, J. Oxygen Plasma Treatment-Enhanced Humidity Sensing Performance of MoS2 Nanoparticles-Anchored Nitrogen-Doped Laser-Induced Graphene. *Sens. Actuators, B* **2024**, *408*, No. 135528.

(26) Zhang, J.; Ren, M.; Wang, L.; Li, Y.; Yakobson, B. I.; Tour, J. M. Oxidized Laser-Induced Graphene for Efficient Oxygen Electrocatalysis. *Adv. Mater.* **2018**, *30* (21), No. 1707319.

(27) Nazeri, M.; Ghalamboran, M.; Grau, G. Laser-Induced Graphene Electrodes for Organic Electrochemical Transistors (OECTs). *Adv. Mater. Technol.* **2023**, *8* (17), No. 2300188.

(28) Lazar, J.; Schnelting, C.; Slavcheva, E.; Schnakenberg, U. Hampering of the Stability of Gold Electrodes by Ferri-/Ferrocyanide Redox Couple Electrolytes during Electrochemical Impedance Spectroscopy. *Anal. Chem.* **2016**, *88* (1), 682−687.

(29) Taurino, I.; Carrara, S.; Giorcelli, M.; Tagliaferro, A.; De Micheli, G. Comparison of Two Different Carbon Nanotube-Based Surfaces with Respect to Potassium Ferricyanide Electrochemistry. *Surf. Sci.* **2012**, *606* (3), 156−160.
(30) Ribeiro, J. A.; Silva, E.; Moreira, P. S.; Pereira, C. M. Electrochemical Characterization of Redox Probes at Gold Screen-Printed Electrodes: Efforts towards Signal Stability. *ChemistrySelect* **2020**, *5* (17), 5041−5048.
(31) Krishnaveni, P.; Ganesh, V. Electron Transfer Studies of a Conventional Redox Probe in Human Sweat and Saliva Bio-Mimicking Conditions. *Sci. Rep.* **2021**, *11* (1), No. 7663.
(32) Kolthoff, I. M.; Tomsicek, W. J. The Oxidation Potential of the System Potassium Ferrocyanide−Potassium Ferricyanide at Various Ionic Strengths. *J. Phys. Chem. A* **1935**, *39* (7), 945−954.
(33) Koç, Y.; Morali, U.; Erol, S.; Avci, H. Investigation of Electrochemical Behavior of Potassium Ferricyanide/Ferrocyanide Redox Probes on Screen Printed Carbon Electrode through Cyclic Voltammetry and Electrochemical Impedance Spectroscopy. *Turk. J. Chem.* **2021**, *45* (6), 1895−1915.
(34) Lister, A. S. 7 - Validation of HPLC Methods in Pharmaceutical Analysis. In *Separation Science and Technology*; Ahuja, S.; Dong, M. W., Eds.; Academic Press, 2005; Vol. *6*, pp 191−217 DOI: 10.1016/S0149-6395(05)80051-0.
(35) Robinson, R. A.; Stokes, R. H. *Electrolyte Solutions: Second Revised ed.*; Courier Corporation, 2002.
(36) Shovan, S. D.; Ringky, S. A.; Islam, A. M.; Islam, S.; Rashid, M. J. Maximizing the Solar Output Power Using Hybrid (CdS/ZnSe) Buffer for CIGS Thin Film Solar Cell. *Phys. Scr.* **2023**, *98* (11), No. 115945.
(37) Ariyoshi, K.; Siroma, Z.; Mineshige, A.; Takeno, M.; Fukutsuka, T.; Abe, T.; Uchida, S. Electrochemical Impedance Spectroscopy Part 1: Fundamentals. *Electrochemistry* **2022**, *90* (10), No. 102007.
(38) Priante, F.; Salim, M.; Ottaviano, L.; Perrozzi, F. XPS Study of Graphene Oxide Reduction Induced by (100) and (111)-Oriented Si Substrates. *Nanotechnology* **2018**, *29* (7), No. 075704.
(39) Wu, J.-B.; Lin, M.-L.; Cong, X.; Liu, H.-N.; Tan, P.-H. Raman Spectroscopy of Graphene-Based Materials and Its Applications in Related Devices. *Chem. Soc. Rev.* **2018**, *47* (5), 1822−1873.
(40) Ferrari, A. C.; Basko, D. M. Raman Spectroscopy as a Versatile Tool for Studying the Properties of Graphene. *Nat. Nanotechnol.* **2013**, *8* (4), 235−246.
(41) Li, C.; Xiong, J.; Zhao, J. Oxygen Plasma Treatment-Enhanced Humidity Sensing Performance of MoS2 Nanoparticles-Anchored Nitrogen-Doped laser-Induced Graphene. *Sens. Actuators, B* **2024**, *408*, No. 135528.
(42) Mendez-Linan, J. I.; Ortiz-Ortega, E.; Jimenez-Moreno, M. F.; Mendivil-Palma, M. I.; Martínez-Guerra, E.; Aguirre-Tostado, F. S.; Martinez-Chapa, S. O.; Hosseini, S.; Madou, M. J. Aging Effect of Plasma-Treated Carbon Surfaces: An Overlooked Phenomenon. *Carbon* **2020**, *169*, 32−44.
(43) Liu, L.; Lei, L.; Zeng, K.; Wu, K.; Yang, N. Surface Chemistry Determined Electrochemical Sensing Performance of Red Phosphorus and Single Walled Carbon Nanotube Composites. *Adv. Funct. Mater.* **2023**, *33* (3), No. 2211335.
(44) Minitha, C. R.; Anithaa, V. S.; Subramaniam, V.; Kumar, R. T. R. Impact of Oxygen Functional Groups on Reduced Graphene Oxide-Based Sensors for Ammonia and Toluene Detection at Room Temperature. *ACS Omega* **2018**, *3* (4), 4105−4112.

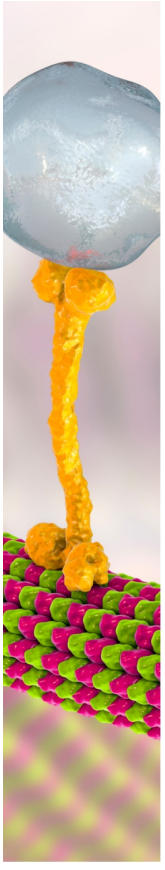

CAS BIOFINDER DISCOVERY PLATFORM™
BRIDGE BIOLOGY AND CHEMISTRY FOR FASTER ANSWERS
Analyze target relationships, compound effects, and disease pathways
Explore the platform
CAS
A division of the American Chemical Society

https://doi.org/10.1021/acsanm.5c02542
ACS Appl. Nano Mater. 2025, 8, 17052−17064